JOURNAL OF APPLIED PHYSICS **115**, 193301 (2014)

Computational study of plasma sustainability in radio frequency micro-discharges

Y. Zhang,[1,2] W. Jiang,[2,3] Q. Z. Zhang,[1] and A. Bogaerts[1,a)]
[1]*Research group PLASMANT, Department of Chemistry University of Antwerp, B-2610 Wilrijk-Antwerp, Belgium*
[2]*School of Physics, Huazhong University of Science and Technology, Wuhan 430074, China*
[3]*Centre for Mathematical Plasma-Astrophysics, Department of Mathematics, Katholieke Universiteit Leuven, B-3001 Leuven, Belgium*

(Received 13 March 2014; accepted 5 May 2014; published online 15 May 2014)

We apply an implicit particle-in-cell Monte-Carlo (PIC-MC) method to study a radio-frequency argon microdischarge at steady state in the glow discharge limit, in which the microdischarge is sustained by secondary electron emission from the electrodes. The plasma density, electron energy distribution function (EEDF), and electron temperature are calculated in a wide range of operating conditions, including driving voltage, microdischarge gap, and pressure. Also, the effect of gap size scaling (in the range of 50-1000 μm) on the plasma sustaining voltage and peak electron density at atmospheric pressure is examined, which has not been explored before. In our simulations, three different EEDFs, i.e., a so-called three temperature hybrid mode, a two temperature α mode, and a two temperature γ mode distribution, are identified at different gaps and voltages. The maximum sustaining voltage to avoid a transition from the glow mode to an arc is predicted, as well as the minimum sustaining voltage for a steady glow discharge. Our calculations elucidate that secondary electrons play an essential role in sustaining the discharge, and as a result the relationship between breakdown voltage and gap spacing is far away from the Paschen law at atmospheric pressure. © *2014 AIP Publishing LLC*.
[http://dx.doi.org/10.1063/1.4878161]

I. INTRODUCTION

Microdischarges (MDs) are plasma sources that allow conventional glow discharges to operate on a continuous basis at gas pressures up to atmospheric pressure by shrinking the dimensions below 1 mm, following the famous pd product (i.e., product of pressure and characteristic gap size).[1,2] In recent years, MDs have gained strong interest as they can indeed produce a stable non-equilibrium plasma at atmospheric pressure. The most remarkable advantages of MDs are the low voltage and power that is necessary to drive the discharge, but the discharge can still be stable at atmospheric pressure and high discharge power densities (100 kW/cm^3). In fact, to maintain a non-equilibrium high pressure plasma in other configurations than a MD is hard or even impossible, because small fluctuations tend to be unstable and trigger a rapid rise in the gas temperature (i.e., transition to a thermal plasma arc). MDs can create a highly reactive environment that contains charged particles, excited species, radicals and photons, and the reduced dimensions enable low-power sources with small footprints suited for integration in microsystems and portable devices. Therefore, atmospheric pressure MDs have become of great importance for fundamental and industrial research in recent years, as they can be used in a broad range of applications,[3–7] such as for material processing, displays, radiation sources, microsatellite propellers, and in biomedical and environmental applications. Furthermore, they may also become of great interest for the chemical industry because they create a highly reactive environment at ambient temperatures and they may open up alternative, highly flexible, environmentally friendly, and energy saving chemical conversion routes.

MDs exist in numerous different configurations such as DC glow discharges,[8,9] dielectric barrier discharges (DBDs),[10,11] and radio-frequency (rf) discharges.[12–16] In particular, atmospheric pressure rf discharges are of great interest, because they show interesting physics, including high plasma density, and they have widespread applications.[17,18] A large variety of rf MDs, operating over a wide range of frequencies,[12,16,19] and with some characteristic discharge dimensions,[13] have been studied.[20] Some unique properties, such as discharge mode transition, the role of highly energetic electrons, and non-equilibrium characteristics, have been demonstrated.[12,13]

However, despite the large number of studies performed on MDs in the past 10 years, the physics and chemistry of MDs are still far from understood. First, these MDs differ from their larger scale, lower-pressure counterparts, as will be illustrated below for the breakdown of pd scaling at different gaps. Second, with micrometer and submillimeter gaps, the role of "boundary dominated" phenomena, such as secondary electron emission (SEE), becomes very important, which can cause the reduction of the required operating voltage. Given these challenges, it is interesting to understand the role of the various operating parameters in MDs, such as the driving voltage, pressure, discharge gap size, and especially the pd scaling and the minimum plasma sustaining voltage.

It is well known that the gas pressure p and the gap size d are key parameters in determining the breakdown voltage, or in explaining how the plasma can be sustained in MDs.

a)Electronic address: annemie.bogaerts@uantwerpen.be

From the Paschen law, the breakdown voltage in a DC-discharge, i.e., the voltage necessary to start a discharge or electric arc, can be predicted as a function of pressure and gap length.[21] In our paper, the breakdown voltage is the voltage necessary to start a 13.56 MHz rf-steady-state-glow-discharge and to sustain the plasma at steady state.

Some groups have studied the breakdown voltage versus pd scaling in a DC discharge model,[1,8,22–25] focusing either on gaps smaller than 50 μm at atmospheric pressure or on gaps larger than 200 μm at a pressure lower than atmospheric. However, due to the complicated physics and the time-consuming numerical simulation processes involved, the pd scaling on atmospheric pressure rf breakdown voltages in MDs with a wide range of gap sizes (50–1000 μm) has not been considered until now, which might open up a new paradigm. Such a computational study is indeed much more time consuming than for a low pressure or DC discharge. In addition, the effect of pressure on the breakdown voltage in rf MDs has also not yet been explored. Therefore, in the present paper, we want to investigate how the pd scaling affects the breakdown voltage in rf MDs sustained by SEE in a gap varying from 50 to 1000 μm. For this purpose, we use an implicit PIC-MC method. First, the effect of various operating parameters, including the driving voltage (50–500 V), the gap size (50–1000 μm), and the pressure (50–760 Torr) on the MD behavior will be presented. Second, the effect of gap size (d) and pressure (p) scaling on the breakdown voltage in MDs at steady state will be examined. Note that we do not only try to address the dependence of the plasma properties on the operating parameters but we also aim to predict the minimum values of these parameters for sustaining the plasma, and especially, we try to find the optimum parameters, including the rf-voltage and gap size, for atmospheric pressure MDs in argon, operating in a stable way in the glow mode. We will show that the resulting discharge behaves like a glow discharge, which is a self-sustaining cold discharge sustained by SEE.

II. DESCRIPTION OF THE MODEL

Numerical studies of MDs can be either based on a fluid model or on a kinetic model, i.e., the PIC-MC method. MDs are generally at non-equilibrium and the electron velocity distribution is typically non-Maxwellian, although most MDs are not far from thermal equilibrium at high pressures. Fluid simulations[1,8] have provided important information about MDs; however, they assumed a Maxwellian electron velocity distribution. It would be more accurate to use the PIC-MC model.[13] On the other hand, the plasma density in MDs can be as high as $10^{23}\,m^{-3}$, and the electron temperature is about 1 eV, which will lead to a small Debye length (in the order of $10^{-4}\sim10^{-5}$ cm) and a high electron oscillation frequency (around $10^{14}\sim10^{15}$Hz). As is well known, an explicit PIC model requires to resolve the Debye length and the electron oscillation frequency, which will lead to a high computational cost several thousands cells and billions of time steps). Indeed, if the spatial grid of the explicit simulation does not resolve the Debye sheath, the particles will be numerically heated, i.e., so-called "self-heating." Moreover, the high pressure makes the situation even worse, because the simulations require a much longer time to reach steady state.

The alternative approach is to adopt an implicit PIC-MC method,[26] which allows us to use much larger space and time steps while keeping the same accuracy. Here, we use a direct implicit method, in which the field equations are derived from direct summation and extrapolation of the equations of particle motion. Our method has been described in detail and tested widely before.[27,28] Therefore, we only briefly summarize it here. In general, the calculation of particle motion, or the so called "particle pushing procedure" is divided into a so-called "first-push"

$$\begin{aligned} \tilde{v}^{n+1/2} &= v^{n-1/2} + \frac{1}{2}\bar{a}^{n-1}\delta t, \\ \tilde{x}^{n+1} &= x^{n} + \frac{1}{2}\tilde{v}^{n+1/2}\delta t, \end{aligned} \tag{1}$$

and a "final-push"

$$\begin{aligned} x^{n+1} &= \tilde{x}^{n+1} + \frac{1}{2}a^{n+1}\delta t^2, \\ v^{n+1/2} &= \tilde{v}^{n+1/2} + \frac{1}{2}a^{n+1}\delta t, \end{aligned} \tag{2}$$

where x^{n+1}, $v^{n+1/2}$, and a^{n-1} are the position, velocity, and averaged accelerations of the macro particles, and tilde is attributed to the intermediate values between the time steps n and n + 1. Furthermore, $a^{n+1} = qE^{n+1}/m$ and $\bar{a}^n$ is used for Eq. (1) and updated by

$$\bar{a}^n = \frac{1}{2}(\bar{a}^{n-1} + a^{n+1}). \tag{3}$$

Between the two pushing procedures, the electric field E^{n+1} at time t^{n+1} is solved by

$$\nabla \cdot [1 + \chi(\vec{x})]\nabla\phi^{n+1} = -\tilde{\rho}^{n+1}, \tag{4}$$

where $\tilde{\rho}^{n+1}$ denotes the charge density calculated at $\tilde{x}^{n+1}$, and $\chi(\vec{x}) = \sum_v \frac{1}{2}\tilde{\rho}_v^{n+1}\frac{q_v}{m_v}\delta t^2$. The $\sum_v$ denotes the summation over all species particles. After the procedures of pushing the particles and solving the electric field, a standard MC procedure is executed.[29] We consider only electron-atom and ion-atom collisions (i.e., electron impact ionization and excitation from the Ar ground state, and electron-Ar and Ar+-Ar elastic collisions), as the ionization degree is never larger than 1% and Coulomb collisions are negligible.[28] The cross sections for these reactions are adopted from Refs. 30–32. In summary, the simulation cycle consists of the following steps: (1) first pushing; (2) weighting; (3) solving the electric field equation; (4) final pushing; and (5) MC process.

A 13.56 MHz rf-voltage source with peak voltages in the range of 50–500 V is used to drive the discharge. Argon gas is used at a temperature of 300 K and the pressure ranges from 50 Torr to 760 Torr. The discharge is sustained between two parallel plate electrodes separated by a gap distance varying from 50 to 1000 μm.

The PIC-MC method in this paper is modified by adding a SEE model. SEE is known as an Auger electron emission

process,[31] and its coefficients depend on many factors, such as the electrode material, the state of the electrode surface (e.g., clean or contaminated), the kind of species and their energy when impacting on the electrode. We have studied the effects of different SEE coefficients, and we found that if the coefficients are not assumed zero, the absolute values of the results are different, but qualitatively the differences are rather small. We assumed a value of 0.2 for the SEE coefficients due to ion and electron impact throughout the paper, which corresponds to a clean stainless steel surface at low energy.[32] As the electron and ion densities increase rapidly due to SEE, a particle merging algorithm is used when the particle number exceeds a certain value. This PIC-MC method is stable over a very broad range of physical and numerical parameters.

In MDs, the fast oscillation modes of electrons are not so much of interest,[8] so we only need to resolve the rf-frequency in time. Moreover, the Debye length does not need to be resolved with this implicit method,[30] so only the sheath needs to be fully resolved in space. This saves us a significant computational cost, and thus it allows us to reach steady state within a reasonable time and to scan the operating parameters over a broad range. The simulation time-step is fixed at 10^{-12} s and the gap space is divided into 128 cells in all cases, i.e., independent from the gap spacing. The initial electron and ion temperatures are 3 eV and 300 K, respectively. In order to reach steady state, we ran the simulations for several thousand rf periods. All the simulation results, such as the electron and ion densities, the electron temperature, the electric field and potential, and the electron energy distribution functions (EEDFs), will be presented by averaging over one rf period after the simulations have reached steady state.

III. DISCHARGE BEHAVIOR IN A WIDE PARAMETER RANGE

A. Effect of applied rf voltage

The effect of rf-voltage on the electron and ion densities is shown in Fig. 1 for two different gap sizes, i.e., 500 μm (upper panels (a)–(c)) and 100 μm (lower panels (d)–(g)), at atmospheric pressure. In all cases, the electron and ion

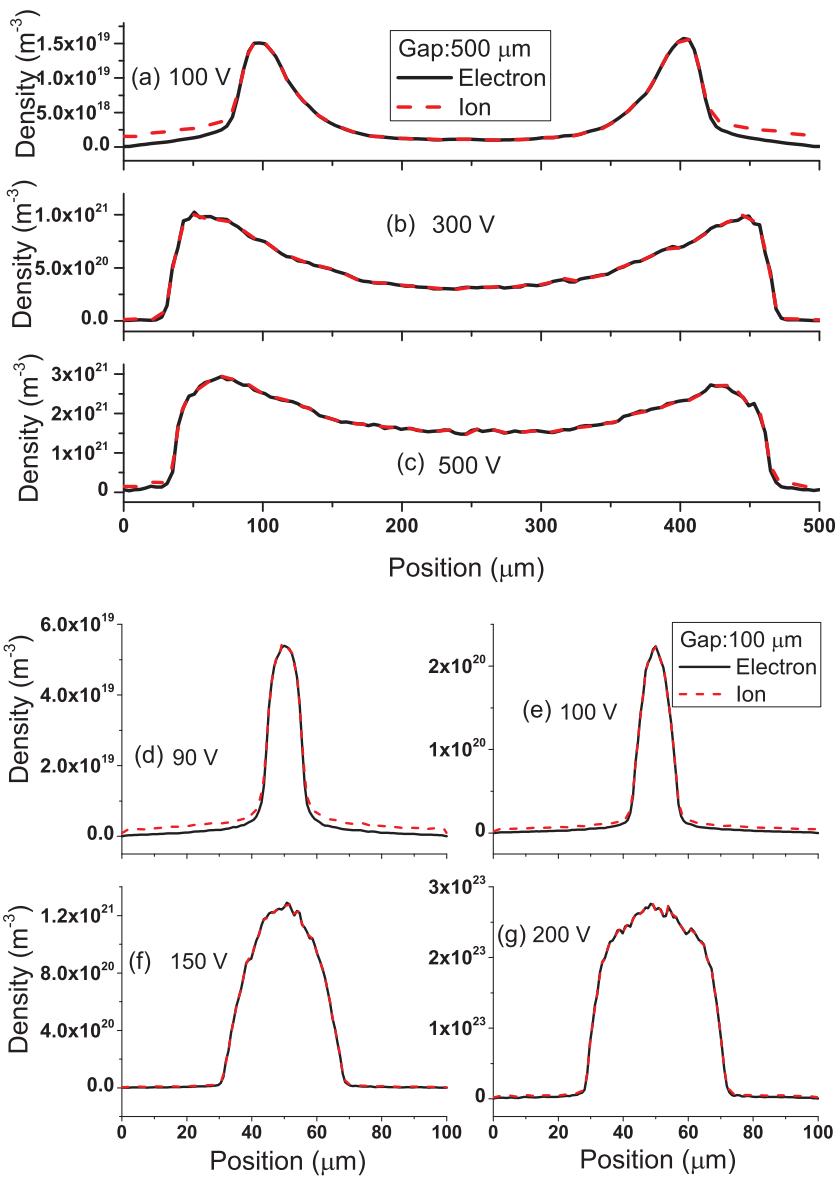

FIG. 1. Electron (solid lines) and ion (dashed lines) density profiles for two different gap sizes, i.e., 500 μm (upper panel, with rf-voltages of 100 V (a), 300 V (b), and 500 V (c)), and 100 μm (lower panel, with rf-voltages of 90 V (d), 100 V (e), 150 V (f), and 200 V (g)), at atmospheric pressure.

densities are more or less equal to each other as expected, except in the sheaths, where the ion density is slightly higher, creating a net positive space charge. The densities rise with applied voltage in both discharge gaps, as expected. Furthermore, the maximum plasma density in the 100 μm gap is significantly larger than in the 500 μm gap for the same rf-voltage (i.e., a difference of one order of magnitude at 100 V, as is clear from Fig. 1). Indeed, the electric field is much higher in the smaller gap at the same voltage, leading to more ionization.

The electron and ion density profiles show two symmetric peaks near the sheath boundary in the case of the 500 μm gap (upper panel), which is similar to experimental observations[33] in a SEE sustaining MD. On the other hand, in the case of the 100 μm gap (lower panel) the density profiles show only a single peak in the center. This will be explained in the following paragraphs.

First, it is important to realize that, despite the high collision frequency at atmospheric pressure, the ions and electrons do not necessarily exhibit a local behavior in a MD. When the discharge is in a so-called hybrid mode[33] (i.e., sustained by SEE), a "local discharge" means that the SEE electrons cannot reach the bulk region and most of them will lose their energy in the sheath. A "nonlocal discharge," on the other hand, means that the SEE electrons can reach or pass through the bulk region and induce ionization in the bulk plasma.

At the discharge gap of 500 μm, it can easily be seen from the density profiles in Figs. 1(a)–1(c) that for an rf voltage of 300 V and 500 V, the MD is nonlocal, while it is local for the rf voltage of 100 V (i.e., steep density peaks at the sheath boundaries and low density in the bulk). In other words, the SEE electrons gain more energy with increasing driving voltage (from 100 V to 300 V and 500 V) and the mean free path of these electrons becomes comparable to or larger than half of the width of the bulk region between the sheath boundaries. Thus, these SEE electrons can reach or pass through the bulk region and give rise to ionization, explaining why the electron and ion densities are reasonably high in the bulk at 300 V and 500 V, while they are almost negligible in the bulk at 100 V. Furthermore, the sheaths occupy a larger portion of the discharge gap when the rf voltage is reduced, which is explained because the electron and ion densities are lower at lower rf voltage. The peak densities are calculated to be 1.5×10^{19}, 10^{21}, and $2.9 \times 10^{21}\,m^{-3}$, respectively, for 100 V, 300 V, and 500 V. Hence, the difference between 100 and 300 V is much larger than between 300 and 500 V, which is again explained by the local vs. non-local behavior. Note that 500 V was found to be the maximum discharge voltage in the 500 μm gap, to avoid the transition from glow to arc discharge in our simulations.

At the discharge gap of 100 μm, the density profiles in Figs. 1(d)–1(g) indicate that the MD is nonlocal at all conditions investigated. Indeed, the gap size is so small that the mean free path of the SEE electrons is typically larger than half of the gap size, and therefore, the SEE electrons can easily enter the bulk region and give rise to ionization, explaining the maximum ion and electron densities in the center. It is clear that the sheaths occupy again a smaller portion of the discharge gap at higher rf-voltages, and hence, the plasma density shows a broader maximum in the discharge center. Moreover, the plasma density becomes much larger upon rising voltage. Indeed, the peak densities are 5.4×10^{19}, 2.2×10^{20}, 1.3×10^{21}, and $2.7 \times 10^{23}\,m^{-3}$, respectively, for 90 V, 100 V, 150 V, and 200 V. Hence, in this case, the difference is very large between 150 and 200 V, as well as between 90 and 100 V. This can be explained because the plasma is sustained in a steady state glow mode between minimum 90 V and maximum 200 V breakdown rf voltage, and in this narrow plasma stability range a small increase in rf voltage leads to a large increase in plasma density. Note that the maximum discharge voltage in the 100 μm gap to avoid the transition to an arc discharge was indeed approximately 200 V in our simulations.

It should be realized that in our PIC-MC model, we adopted a 1D electrostatic model, and we do not consider the magnetic field induced by the plasma current. Moreover, we also keep the density and temperature of the background gas fixed. Both assumptions are valid as long as the total ionization rate is not very high (i.e., ionization degree $< 10\%$) and the gas heating is not significant, which is indeed the case for the MDs operating in the glow regime. However, our model cannot be used to describe the discharge in the arc regime, where the magnetic field and gas heating cannot be neglected. Therefore, the upper plasma density limit of our simulations is about 10^{22}–$10^{24}\,m^{-3}$ at the operating conditions under study. Beyond these values, the plasma density would increase rapidly, and the calculations would collapse shortly. Hence, this also sets the upper limit of the applied rf voltage, which is indeed around 500 V in the gap of 500 μm and 200 V in the gap of 100 μm at atmospheric pressure.

Finally, it is striking that in the 100 μm gap the sheaths occupy more than half of the discharge gap, and even more at the rf voltages of 90 and 100 V. It has been reported[7,13] that when the sheaths are larger than half of the gap size, the overall time-averaged electron and ion densities do not give rise to an electrically neutral plasma. This will be further discussed explicitly in Sec. III B.

Figure 2 presents the time-averaged potential distributions, for the same gap sizes and rf voltages as in Fig. 1. As is well known, with increasing rf-voltage, the plasma potential increases in both gaps. Furthermore, it is clear that the sheaths become thinner at higher rf voltages, as could also be deduced from Fig. 1 above. Due to the relatively low plasma potentials (several tens of V), the avalanche induced by the SEE electrons in the discharge will be limited. In other words, the SEE electrons will be able to give rise to only a few ionization collisions on their journey from electrode to the bulk plasma, before they become thermal.

In order to examine the corresponding electron kinetics, we plot the space-time-averaged EEDFs and the electron temperature profiles in Fig. 3, for the different rf voltages, and the two different gaps. As the gap size decreases from 500 μm to 100 μm, a transition of the electron heating mode is observed. Indeed, the EEDFs change from a three-temperature distribution (hybrid mode) in the 500 μm gap (at least in the case of 100 and 500 V) to a two-temperature distribution (in the case of 150 and 200 V) and a

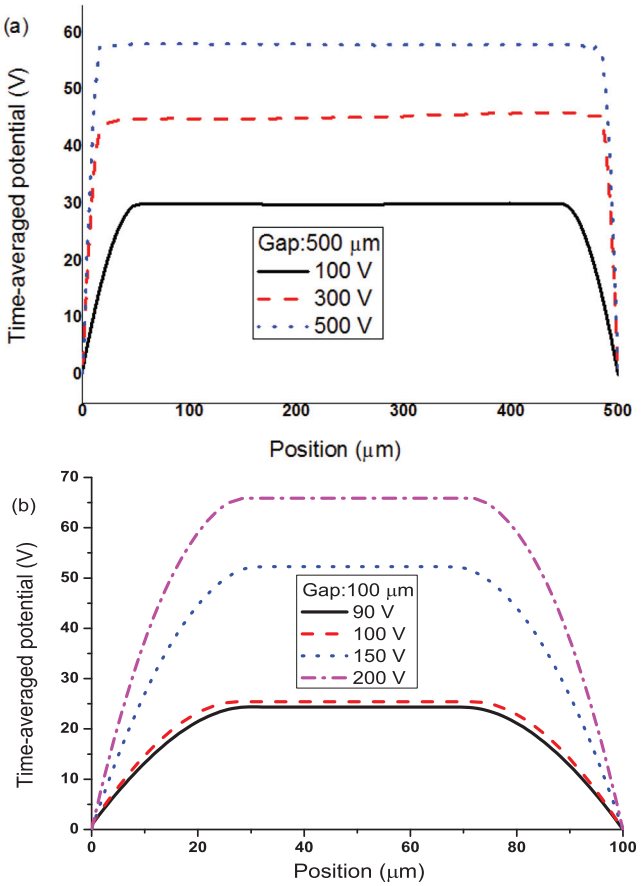

FIG. 2. Time-averaged potential distributions for a gap size of 500 μm (a) and 100 μm (b), and different rf voltages (see legend).

one-temperature distribution (at 90 and 100 V) in the 100 μm gap (γ mode), as is shown in Figs. 3(a) and 3(b).

The three electron groups that can be identified in the EEDFs of Fig. 3(a), in the case of 100 and 500 V, correspond to low-energy (<1.5 eV), mid-energy (between 1.5 and 12 eV), and high-energy (>12 eV) electrons. At 300 V, a two-temperature distribution (i.e., α mode discharge) is observed in Fig. 3(a), with two electron groups corresponding to low energy (<2.5 eV) and relatively high-energy (>2.5 eV), and the SEE induced γ mode seems to be negligible. This is also clearly illustrated by the dashed line in Fig. 3(c), where no peaks in the electron temperature are observed at the sheath boundaries for the 300 V case. Note that this α mode dominated two-temperature EEDF, as obtained in the 500 μm gap at 300 V, is essentially different from the γ mode two-temperature EEDFs, obtained in the 100 μm gap at 150 and 200 V (see Figure 3(b)). Indeed, in a two-temperature α mode, the EEDF is dominated by low energy bulk electrons, whereas in a two-temperature γ mode, the EEDF is dominated by the energetic SEE electrons, which are rapidly accelerated across the sheath due to the high electric field. The two electron groups that can be identified in Fig. 3(b) at 150 and 200 V indeed correspond to mid-energy (between 0.2 and 1.3 eV) and relatively high-energy (>1.3 eV), which is different from the two electron groups identified in Fig. 3(a); see above. In addition, the one electron group in Fig. 3(b) at 90 and 100 V corresponds to relatively high energy (>0.2 eV).

The question now arises why the 500 μm gap at 100 V and 500 V results in a hybrid mode (three-temperature electron distribution), whereas the 500 μm gap at 300 V yields a

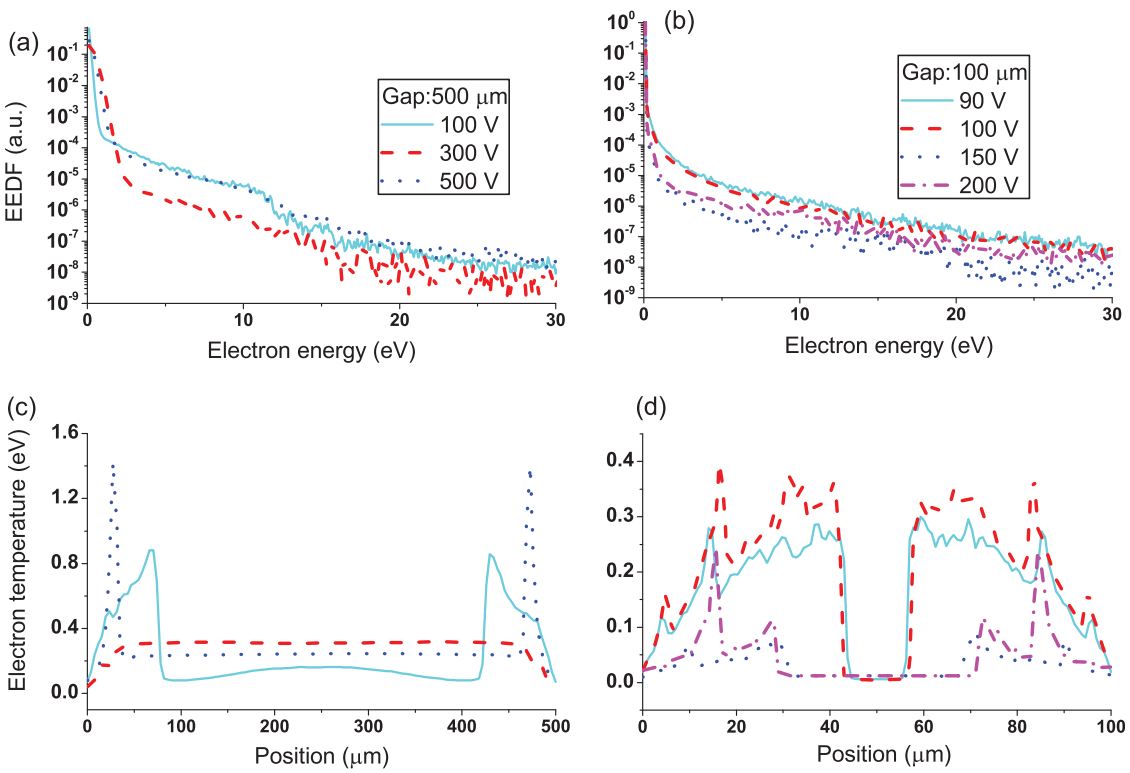

FIG. 3. Space-time-averaged EEDFs ((a) and (b)) and electron temperature profiles ((c) and (d)), for a gap size of 500 μm ((a) and (c)) and 100 μm ((b) and (d)) for different rf-voltages (see legend).

two-temperature α mode distribution, and the 100 μm gap gives a two/one-temperature γ mode distribution at all voltages. The answer for the different behavior at 300 V in the 500 μm gap can be found when comparing Figs. 1(b) and 1(c). Indeed, at 300 V, there is almost no difference between the ion and electron densities in the sheaths, resulting in a weak electric field, whereas at 500 V, the ion density is somewhat higher than the electron density, giving rise to a positive space charge and hence a stronger electric field in the sheath. This could also be seen in Fig. 2(a). This stronger electric field implies that more SEE electrons can be accelerated and give rise to ionization, explaining the hybrid mode at 500 V, whereas the weaker electric field at 300 V explains the α mode. The reason why the 100 μm gap yields a γ mode distribution can be explained because the sheaths occupy a larger portion of the gap and SEE becomes the main source of the plasma electrons.

As shown in Figs. 3(c) and 3(d), the electron temperatures exhibit also quite different profiles for the 500 μm and 100 μm discharge gaps, because of the mode transition demonstrated above. The peak electron temperature values are 0.9, 0.3, and 1.4 eV, respectively, for 100 V, 300 V, and 500 V in the 500 μm gap, whereas the peak electron temperature values are 0.3, 0.4, 0.09, and 0.2 eV, respectively, for 90 V, 100 V, 150 V, and 200 V in the 100 μm gap. The maximum electron temperature in the 500 μm gap is typically larger than in the 100 μm gap. For instance, at the same driving voltage of 100 V, the maximum electron temperature is 0.9 eV in the 500 μm gap and only 0.4 eV in the 100 μm gap. The reason is that the plasma potential in the 500 μm gap is larger than in the 100 μm gap for 100 V. Indeed, in the γ mode discharge, the SEE electrons are accelerated to high energy by the potential drop in the sheath. This also explains why the maximum electron temperature in the 500 μm gap at 300 V is so much lower. The maximum electron temperature at 150 V and 200 V in the 100 μm gap is lower, because in the sheaths the ion and electron densities show a quasi-neutral trend.

It is notable that there is a very strong temperature gradient (with a slope almost infinite) in the temperature profiles for all γ mode cases, as shown in Figs. 3(c) and 3(d), near the sheath edge. This is a natural result for atmospheric pressure discharges, as the pressure is high and many collisions take place, so most of the electrons can only be heated in the sheath. In the bulk plasma, the electrons cannot be heated by the rf electric field and will be cooled by the collisions, so most of them will rapidly lose their energy, leading to a significant temperature drop near the inner sheath edge.

In the hybrid mode (Fig. 3(c): 100 and 500 V) or the γ mode (Fig. 3(d)), the electron temperatures exhibit a saddle-like profile, with maximum values in the sheaths and minima in the bulk plasma. This can be explained because the electron impact ionization is mainly induced by the SEE beam electrons from the electrodes. Therefore, the electron temperature in the sheaths can show several peaks, which is especially obvious in Fig. 3(d). These peaks correspond to energy gain from the electric field in the sheaths, followed by energy loss due to (ionization or excitation) collisions. On the other hand, the α mode (i.e., in the 500 μm gap at 300 V; see dashed line in Fig. 3(c)) is characterized by a gradually increasing electron temperature inside both sheaths towards a constant value in the bulk discharge region. This is because the bulk electron impact ionization dominates in this case. This also explains why the bulk electron energy is larger at 300 V in the 500 μm gap than at 100 V and 500 V, because of the α heating mode.

B. Effect of gap size

The effect of gap size on the electron and ion densities at an rf-voltage of 100 V and atmospheric pressure is shown in Figs. 4(a)–4(d). As the gap size decreases, the sheaths occupy a larger portion of the discharge gap. However, the neutral bulk discharge region is always sustained at all gaps, even at the smallest gaps of 50 and 200 μm, where the

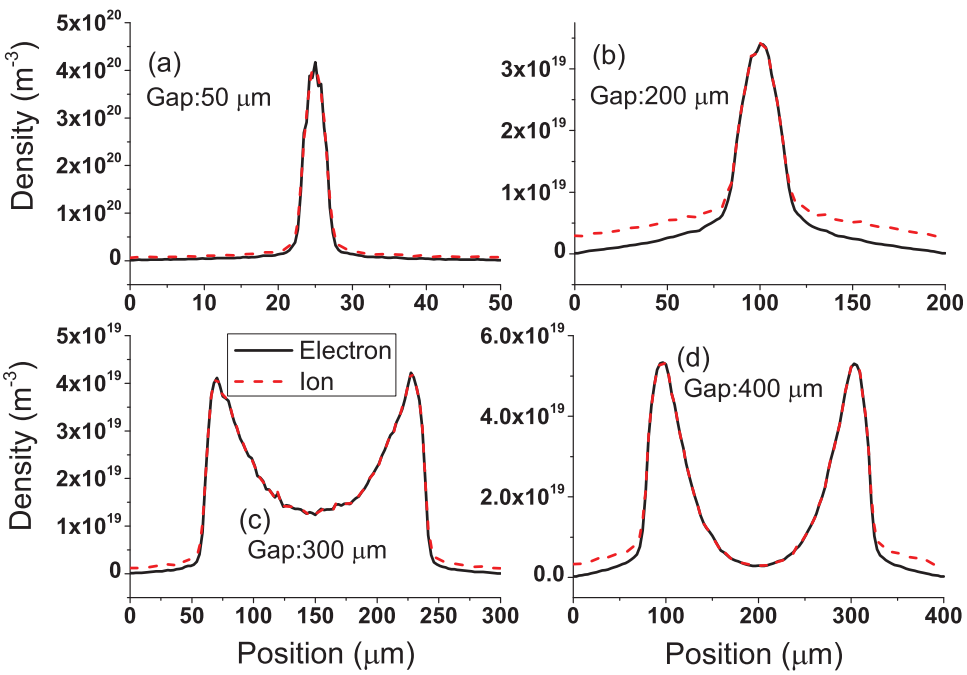

FIG. 4. Electron (solid lines) and ion (dashed lines) density profiles at an rf-voltage of 100 V, for a gap size of 50 μm (a), 200 μm (b), 300 μm (c), and 400 μm (d), at atmospheric pressure.

sheaths are larger than half of the discharge gap. This is in contrast with the simulations of Refs. 7 and 13, where no quasi-neutral bulk region was obtained for the time-averaged bulk density. However, we believe it is necessary that the time-averaged density forms a neutral bulk region, when the simulations reach a steady state.

The plasma densities show a single steep peak in the center in the case of the 50 and 200 μm discharge gaps (Figs. 4(a) and 4(b)), while the densities appear in two symmetric peaks near the sheaths in the case of the 300 and 400 μm gaps (Figs. 4(c) and 4(d)). The peak densities are 4×10^{20}, 3.4×10^{19}, 4×10^{19}, and $5 \times 10^{19}\,m^{-3}$, respectively, for the 50, 200, 300, and 400 μm gaps. Hence, the 50 μm gap results in the highest density. The density profiles can be understood from the mean free path for ionization(s) of the SEE electrons, which is in the order of $\sim$100 μm, depending on pressure, but also on the sheath width and the potential drop in the sheaths. If s is smaller than half of the discharge gap (d/2), two peaks in the density profile appear near the sheaths, whereas if s is larger than or equal to half of the discharge gap (d/2) only a single peak in the center of the bulk region is found, because the two density peaks induced by SEE electrons originating from both electrodes overlap.

In other words, at the 50 and 200 μm gaps, the electrons are not in local equilibrium with the electric fields in the sheaths, because the SEE electrons are accelerated in the sheaths. On the other hand, at the 300 and 400 μm gaps, the electrons are in local equilibrium with the sheath electric fields, even if the SEE electrons are accelerated in the sheaths, since these gap sizes are larger than twice the SEE electron mean free path for ionization. This explains why the discharges at the 300 and 400 μm gaps exhibit a local density distribution.

The space-time averaged EEDFs, recorded for the four different discharge gaps, are shown in Fig. 5(a), for the same rf-voltage of 100 V and atmospheric pressure. The corresponding electron temperature profiles are plotted in Figs. 5(b)–5(e). When the gap size increases, the low-energy electron population increases and the high-energy electron population decreases. The EEDFs are characterized by a three-temperature distribution (i.e., hybrid mode) in the case of the 200 μm, 300 μm, and 400 μm gaps. The three electron groups correspond to low-energy ($<$0.4 eV), mid-energy (between 0.4 and 14 eV), and high-energy ($>$14 eV). The low-energy electron group is induced by the bulk heating, the high-energy electron group is generated by the SEE electrons, which can obtain high energy in the sheaths, and the mid-energy group is created by ionization from the high-energy SEE electrons in the sheaths. In the case of the 50 μm gap, on the other hand, only a two-temperature distribution (γ mode) is found, corresponding to mid-energy electrons ($<$0.2 eV) created from ionization of the SEE electrons and relatively high-energy electrons ($>$0.2 eV) corresponding to the SEE electrons accelerated in the sheaths.

Figs. 5(b)–5(e) show that the electron temperature in the sheaths is much higher than the bulk electron temperature and can show several peaks, which indicates the prevalence of the γ mode, in agreement with experiments.[33] In the plasma bulk, the electron temperature is lower than 0.1 eV, for all discharge gaps investigated, but it increases with increasing gap size, due to the transition from a pure γ mode to a hybrid mode.

The peak temperature values are 0.2, 0.9, 0.3, and 0.6 eV, respectively, for the 50 μm, 200 μm, 300 μm, and 400 μm gaps. The large difference between the 50 μm and 200 μm gaps is due to the strong electric field induced by the large difference in electron and ion densities in the sheaths in the 200 μm gap [see Fig. 4(b)]. The same explanation also holds for the difference between the 300 μm and 400 μm gaps [see Fig. 4(d)].

C. Effect of pressure

Up to now, we have only considered the MD behavior at atmospheric pressure. However, MDs can also operate at reduced pressure, and the effect of gas pressure on the electron densities in the 100 μm gap at an rf-voltage of 100 V is shown in Fig. 6. The electron density profiles are similar at all pressures, with a single peak in the bulk center. In general, the electron density increases with pressure from 100 Torr to 760 Torr, which is logical. However, at 50 Torr the electron density is higher than at 100 and 300 Torr. This can be explained because at this low pressure some of the SEE electrons that are accelerated in the sheath can not only enter the bulk plasma but also reach the opposite sheath and thus they can be further heated there, and induce more ionization, explaining the higher density. The additional heating can also be seen from Fig. 7(b), as the electron temperature at 50 Torr is significantly larger than at the other pressures investigated.

The space-time-averaged EEDFs and the electron temperature profiles at the same conditions are presented in Figs. 7(a) and 7(b). As is clear from Fig. 7(a), the five EEDFs show the same profile with a two temperature distribution, mainly dominated by the high-energy electrons, which is a typical feature of the γ mode. This can also be deduced from the electron temperature profiles (see Fig. 7(b)), which are characterized by several peaks in the sheaths, which are much higher than the values in the bulk plasma. Furthermore, the high energy tail of the EEDFs and the electron temperature almost monotonically decrease upon increasing pressure, which is logical, because of the higher energy loss due to collisions.

IV. BREAKDOWN VOLTAGE VS GAP SIZE AND PRESSURE

In the above sections, we have investigated the plasma characteristics in a wide range of voltages, gap sizes, and pressures. Now, we will focus on the breakdown voltage as a function of pressure and gap spacing, because this is of great interest for practical applications.

The effect of gap size scaling on the breakdown voltage and on the peak electron density (at this breakdown voltage) is plotted in Figs. 8(a) and 8(c), for atmospheric pressure. In addition, the effect of pressure on the breakdown voltage and on the peak electron density at a fixed gap of 100 μm is illustrated in Figs. 8(b) and 8(d). The breakdown voltage shows a

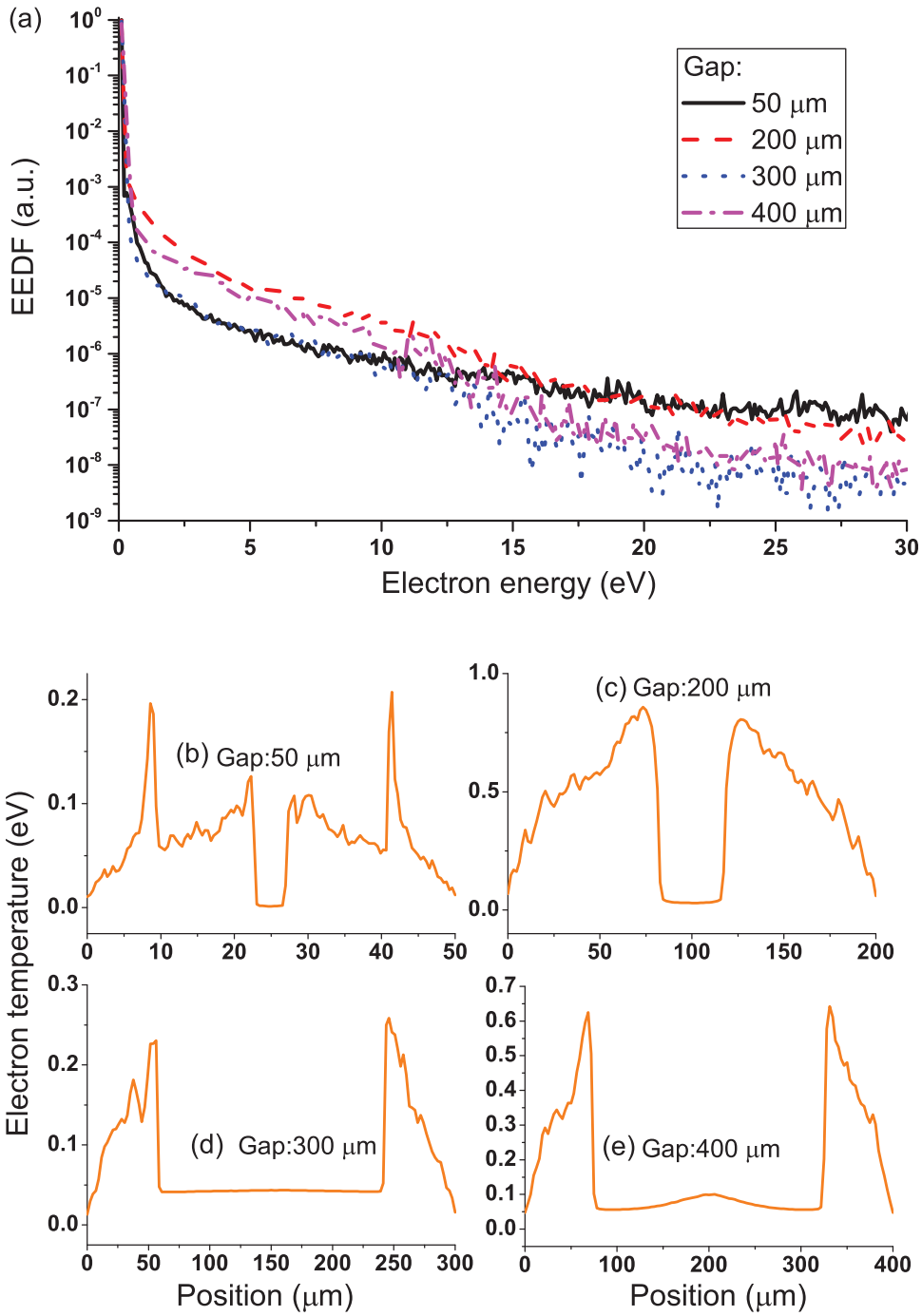

FIG. 5. Space-time-averaged EEDF (a) and electron temperature profiles ((b)–(e)), for an rf voltage of 100 V and different gap sizes at atmospheric pressure.

strongly non-monotonic trend upon increasing gap size, as shown in Fig. 8(a). Indeed, it first increases rapidly from 50 V at 50 μm to 90 V at 100 μm, then it decreases rapidly to again 50 V at 280 μm, and finally it increases slowly to 85 V at 1000 μm. Hence, both the gaps of 50 μm and 280 μm give rise to a minimum breakdown voltage of 50 V at atmospheric pressure. This can again be explained by comparing the mean free paths for ionization of the SEE electrons and the gap spacing, as discussed in Sec. III B. Indeed, the mean free path of the SEE electrons is around 100 μm, so when the gap spacing is larger than twice the mean free path (i.e., 200 μm in this case), the minimum breakdown voltage is similar to the normal Paschen law, which has a minimum at about 250 μm for argon.[21] This means that the electrons accelerated in one sheath will not affect the other sheath. However, when the gap spacing is reduced, and becomes comparable or smaller than the mean free path, the electrons can pass through the bulk plasma, and are further heated in the opposite sheath, which significantly reduces the breakdown voltage and increases the corresponding plasma density.

As illustrated in Fig. 8(b), when varying the gas pressure from 50 to 760 Torr at a gap of 100 μm, the breakdown voltage shows a broad valley with a minimum value of 70 V at a pressure of 200 Torr. This behavior is in satisfactory agreement with the Paschen curve, although the minimum voltage is much lower than those in the Paschen curve of argon (i.e., 150 V).[21] This may be attributed to the important role of SEE in the MD plasmas under study. In fact, our results for

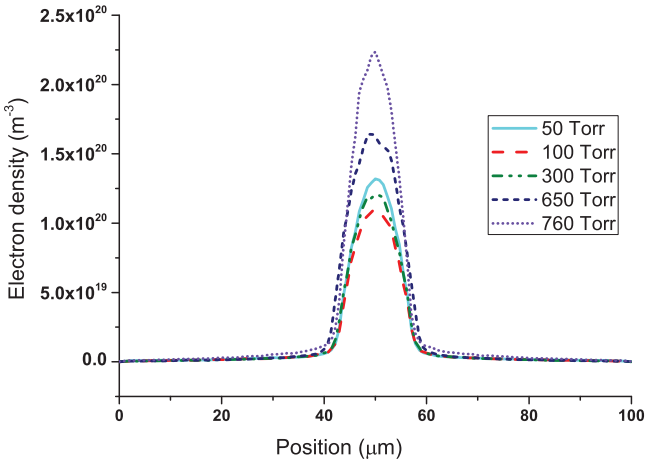

FIG. 6. Electron density profiles at an rf-voltage of 100 V and a gap size of 100 μm, at 5 different pressures.

an rf MD should not be compared quantitatively with the Paschen curve in a DC discharge. Indeed, if there are no SEE electrons, our calculations predict that there will be no stable discharge at such a small gap spacing (<500 μm). Hence, the fact that the V-pd curves for MDs are different from the conventional Paschen law is the natural result of the finite size effect: as the ionization mean free path is comparable to the gap spacing, only a few ionization collisions and no avalanche process can occur in MDs.

Note that the obtained breakdown voltages in the entire range of discharge gaps (50–1000 μm) and pressures (50–760 Torr) are quite small (i.e., not larger than 90 V), which is beneficial in terms of energy considerations. The reason is that these MDs are sustained by SEE. This information can be useful to determine the minimum voltages in

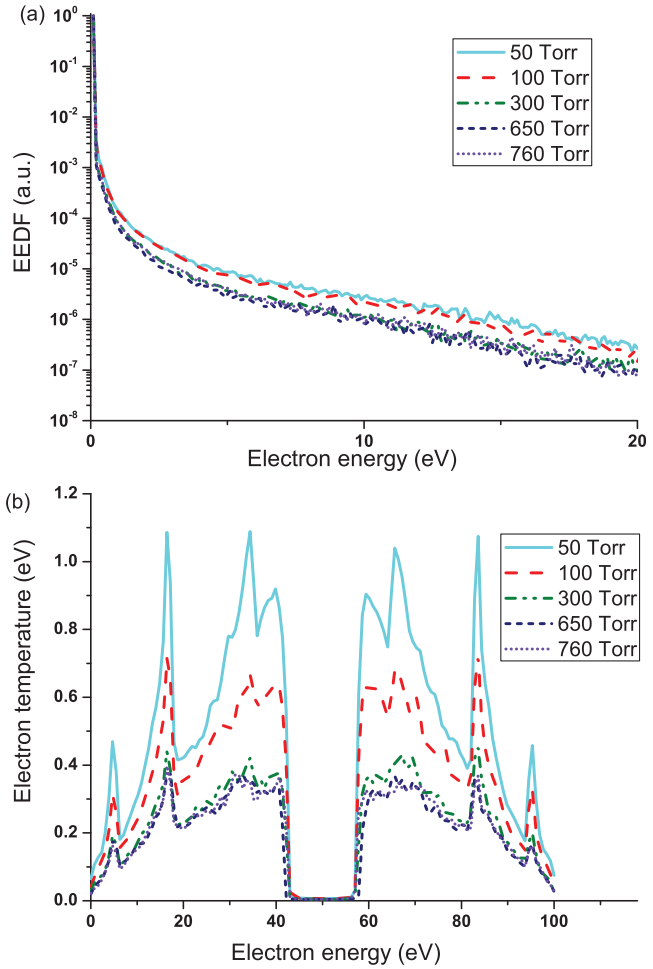

FIG. 7. Space-time averaged EEDF (a) and electron temperature profiles (b) at an rf-voltage of 100 V and a gap size of 100 μm, at 5 different pressures.

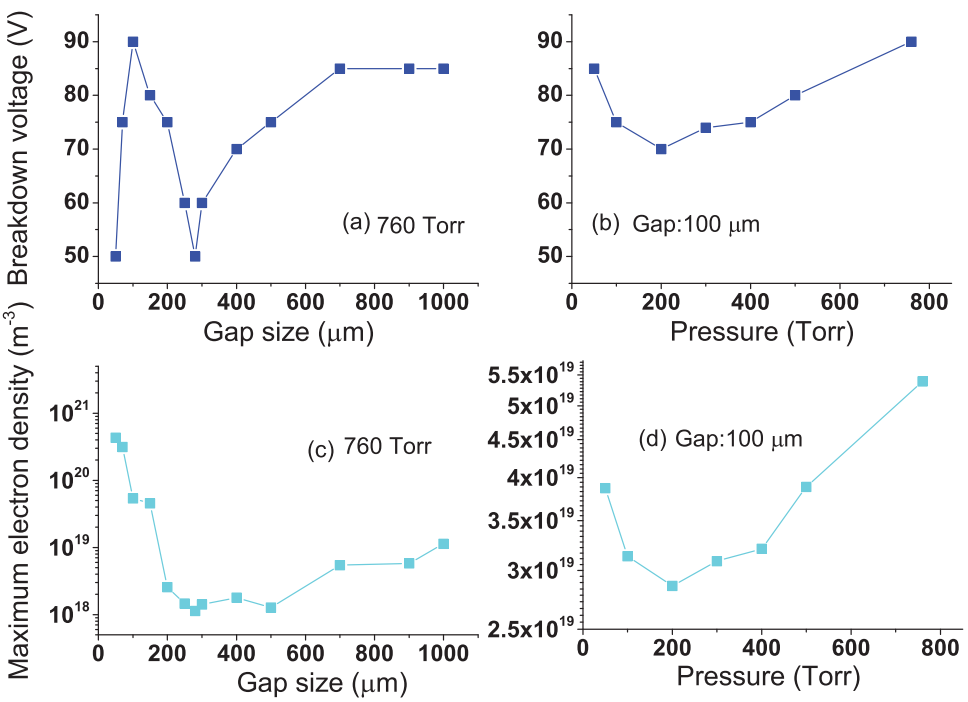

FIG. 8. Breakdown voltage ((a) and (b)) and peak electron density at this breakdown voltage ((c) and (d)), as a function of gap size at atmospheric pressure ((a) and (c)), and as a function of pressure at a gap size of 100 μm ((b) and (d)).

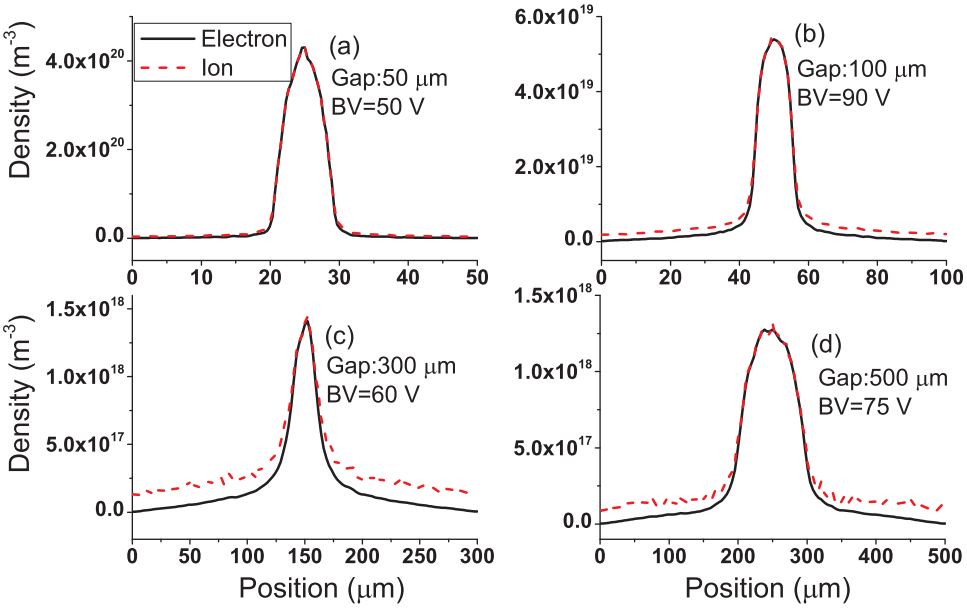

FIG. 9. Electron (solid lines) and ion (dashed lines) density profiles at atmospheric pressure for different gap sizes and their corresponding breakdown voltages (BV), as indicated by the legends.

micro-channel plasma generation and micro-plasma sources, as well as to predict the critical dimensions in micro-plasma devices, for engineering developments of MDs. Fig. 8(c) illustrates that the peak electron density, obtained at the breakdown voltage, decreases very steeply with increasing gap size, i.e., from $4.5 \times 10^{20}\,\mathrm{m}^{-3}$ at a 50 μm gap to $1.1 \times 10^{18}\,\mathrm{m}^{-3}$ at a 280 μm gap, in the case of 760 Torr, and then it slightly increases again to $1.2 \times 10^{19}\,\mathrm{m}^{-3}$ at a 1000 μm gap. The reason is that the electron density is not only determined by the gap size but also depends on the applied driving voltage, hence the breakdown voltage in this case. Indeed, the electron density increases with the electric field (due to more ionization collisions), and the latter is determined from the ratio of the breakdown voltage over the gap size. From 50 to 100 μm, the gap size is dominant in determining the electric field, explaining why the peak electron density decreases quickly with increasing gap size. At large gaps, the breakdown voltage dominantly determines the electric field, explaining why the peak electron density increases slowly with increasing gap size. Furthermore, when varying the pressure at a constant gap size of 100 μm (see Fig. 8(d)), the peak electron density exhibits a minimum value of $2.7 \times 10^{19}\,\mathrm{m}^{-3}$ at 200 Torr. This corresponds to the pressure of the minimum breakdown voltage (cf. Fig. 8(b)). Indeed, this lower voltage results in a lower electric field, at constant gap size, and hence in a lower electron density.

Finally, the spatial distributions of the electron and ion densities at atmospheric pressure and four different gaps (i.e., 50 μm, 100 μm, 300 μm, and 500 μm) and at their corresponding breakdown voltages (i.e., 50 V, 90 V, 60 V, and 75 V) are shown in Figs. 9(a)–9(d). In contrast to the results shown in Fig. 4 above, a single peak in the density distribution is now observed in all cases. Indeed, the double peak distribution results from the SEE dominated discharge, but the breakdown voltage is insufficient to induce a strong SEE and this explains why only a single peak is observed, even at the larger gaps of 300 μm and 500 μm.

V. CONCLUSION

A direct implicit PIC-MC method is applied to study an rf argon MD operating in the glow discharge regime. In this method, the field equations are derived from the direct summation and extrapolation of the Newton equations describing the particle movement. This method allows to use much larger space and time steps while keeping the accuracy, and therefore it reduces the computational cost and self-heating, which is very important for the simulation of atmospheric pressure rf discharges at steady state. It has been demonstrated that this method is stable over a broad range of operating parameters.

First the electron and ion densities, the EEDFs, and the electron temperature profiles are presented in a wide range of operating conditions, i.e., voltages of 50–500 V, a gap size of 50–1000 μm, and a gas pressure in the range of 50–760 Torr, to obtain a better insight in the general plasma behavior. Our calculations predict that at atmospheric pressure the maximum discharge voltage to avoid a transition from glow to arc regime is equal to 500 V for a 500 μm discharge gap, whereas it is around 200 V for a discharge gap of 100 μm.

When the SEE electron mean free path for ionization (s) is smaller than half of the discharge gap (d), as in the case for a discharge gap of 300 μm and above, two electron (and ion) density peaks near the sheath boundaries are observed. On the other hand, when s is equal to or larger than d/2, as in the case for a discharge gap of 200 μm and lower, only a single steep density peak in the center of the bulk region is found.

Furthermore, at atmospheric pressure and a discharge gap of 500 μm, the EEDFs exhibit a three-temperature distribution at 100 V and 500 V, which points towards a so-called "hybrid mode," i.e., a combination of α mode and (dominant) γ mode. On the other hand, at 300 V, the EEDFs show a two-temperature distribution, corresponding to the α-mode, which is attributed to its quasi-neutral plasma density in the

sheaths, giving rise to only a weak electric field and therefore limited electron heating in the sheaths. At a gap size of 100 μm, the EEDF is characterized by a two-temperature distribution, corresponding to the γ-mode, in the entire range of voltages and pressures investigated. The fact that the EEDFs are so much dependent on gap size, besides their dependence on pressure and voltage, can be exploited as a manner for engineering energetic electrons in MDs.

Second, a detailed study is performed of the effect of gap size and pressure on the plasma breakdown voltage, in order to elucidate the different pd scaling on the breakdown voltage in a steady state atmospheric pressure rf MD (with a gap ranging from 50 to 1000 μm), compared to the classical Paschen law, valid for DC discharges at larger gaps or lower pressure. Our calculations predict that at atmospheric pressure, there exist two gap sizes, i.e., 50 μm and 280 μm, which correspond to the minimum breakdown voltage of 50 V, whereas the breakdown voltage is maximum (i.e., 90 V) at a gap of 100 μm. Note that the obtained breakdown voltages in a wide range of discharge gaps (i.e., 50–1000 μm) and pressures (50–760 Torr) are below 90 V. This illustrates that (atmospheric pressure or lower pressure) rf MDs in the glow regime can be operated in an energy efficient manner, which is of crucial importance as energy considerations become more and more critical for many applications, including chemical processing and the synthesis of nanostructures.

ACKNOWLEDGMENTS

Y. Zhang and W. Jiang gratefully acknowledge the Belgian Federal Science Policy Office and the China Scholarship Council for financial support. The calculations were performed using the Turing HPC infrastructure at the CalcUA core facility of the Universiteit Antwerpen, a division of the Flemish Supercomputer Center VSC, funded by the Hercules Foundation, the Flemish Government (department EWI), and the Universiteit Antwerpen.

[1]M. J. Kushner, J. Appl. Phys. **95**, 846 (2004).
[2]P. Bruggeman and R. Brandenburg, J. Phys. D: Appl. Phys. **46**, 464001 (2013).
[3]J. W. Frame, D. J. Wheeler, T. A. DeTemple, and J. G. Eden, Appl. Phys. Lett. **71**, 1165 (1997).
[4]I. Kieft, E. vd Laan, and E. Stoffels, New J. Phys. **6**, 149 (2004).
[5]D. Mariotti and R. M. Sankaran, J. Phys. D: Appl. Phys. **43**, 323001 (2010).
[6]D. Janasek, J. Franzke, and A. Manz, Nature **442**, 374 (2006).
[7]J. J. Shi and M. G. Kong, Phys. Rev. Lett. **96**, 105009 (2006).
[8]M. J. Kushner, J. Phys. D: Appl. Phys. **38**, 1633 (2005).
[9]S. G. Belostotskiy, T. Ouk, V. M. Donnelly, D. J. Economou, and N. Sadeghi, J. Appl. Phys. **107**, 053305 (2010).
[10]S. L. Suib, S. L. Brock, M. Marquez, J. Luo, H. Matsumoto, and Y. Hayashi, J. Phys. Chem. B **102**, 9661 (1998).
[11]R. Li, Q. Tang, S. Yin, and T. Sato, Appl. Phys. Lett. **90**, 131502 (2007).
[12]H. Kim and J. Lee, Phys. Rev. lett. **93**, 085003 (2004).
[13]F. Iza, J. K. Lee, and M. G. Kong, Phys. Rev. Lett. **99**, 075004 (2007).
[14]F. Iza and J. Lee, Comput. Phys. Commun. **177**, 72 (2007).
[15]K. McKay, D. X. Liu, M. Z. Rong, F. Iza, and M. G. Kong, Appl. Phys. Lett. **99**, 091501 (2011).
[16]H. Kwon, I. Won, and J. Lee, Appl. Phys. Lett. **100**, 183702 (2012).
[17]V. A. Godyak and R. B. Piejak, Phys. Rev. Lett. **65**, 996 (1990).
[18]V. A. Godyak, R. B. Piejak, and B. M. Alexandrovich, Plasma Sources Sci. Technol. **1**, 36 (1992).
[19]H. Kwon, H. Kim, I. Won, H. W. Lee, H. Shin, and J. Lee, Phys. Plasmas **20**, 023506 (2013).
[20]K. McKay, F. Iza, and M. Kong, Euro. Phys. J. D **60**, 497 (2010).
[21]Y. P. Raizer, V. I. Kisin, and J. E. Allen, *Gas Discharge Physics* (Springer-Verlag, Berlin, 1991), Vol. 1.
[22]M. Radmilovic-Radjenovic and B. Radjenovic, IEEE Trans. Plasma Sci. **35**, 1223 (2007).
[23]W.-L. Fan, Z.-M. Sheng, W.-M. Wang, Y.-Q. Cui, X.-X. Zhong, Y.-T. Li, and J. Zhang, J. Phys. D: Appl. Phys. **46**, 475208 (2013).
[24]S. G. Belostotskiy, V. M. Donnelly, and D. J. Economou, Plasma Sources Sci. Technol. **17**, 045018 (2008).
[25]J. Wang and G. Loew, in *Proceedings of Joint School RF Engineering for Accelerators*, 1997.
[26]G. Lapenta, J. U. Brackbill, and P. Ricci, Phys. Plasmas **13**, 055904 (2006).
[27]H.-y. Wang, W. Jiang, and Y.-n. Wang, Plasma Sources Sci. Technol. **19**, 045023 (2010).
[28]W. Jiang, H.-y. Wang, Z.-h. Bi, and Y.-n. Wang, Plasma Sources Sci. Technol. **20**, 035013 (2011).
[29]K. Nanbu, IEEE Trans. Plasma Sci. **28**, 971 (2000).
[30]M. A. Lieberman and A. J. Lichtenberg, *Principles of Plasma Discharges and Materials Processing* (Wiley, 2005).
[31]M. Furman and M. Pivi. Phys. Rev. ST Accel. Beams **5**, 124404 (2002).
[32]A. V. Phelps and Z. Lj. Petrovic, Plasma Sources Sci. Technol. **8**, R21 (1999).
[33]D. Schroder, S. Burhenn, D. Kirchheim, and V. Schulz-von der Gathen, J. Phys. D: Appl. Phys. **46**, 464003 (2013).